Modeling Resistance Spot Welding Electrode Life

S. S. Babu, M. L. Santella, and W. Peterson[†]
Oak Ridge National Laboratory, Oak Ridge, Tennessee
[†]Edison Welding Institute, Columbus, Ohio

ABSTRACT

Electrode deterioration by deformation and chemical reaction during resistance spot welding of zinc coated steels is a well-known problem. In the first part of the research, electrode degradation by a deformation mechanism was considered. Analytical expressions of stress-strain characteristics as a function of temperature, degradation of material properties with number of spot welds, and variation of peak temperature at the electrode surface were coupled to predict the growth of electrode face diameter as a function of number of spot welds. The predictions were compared with experimental measurements and showed good agreement. In the next step, electrode degradation by chemical reaction was considered. Diffusion controlled growth models indicated that the solid-state diffusion during a typical thermal cycle of one spot weld is negligible compared to dissolution of copper into liquid zinc.

INTRODUCTION

The zinc used in corrosion protection coatings on carbon steels accelerates the deterioration of copper-alloy resistance spot welding electrodes compared to welding bare steels. The Zn alters the electrical, thermal, and mechanical properties of the steels sheets. Zinc is more electrically and thermally conductive than steel [1]. It is also softer than steel, and it conforms better to electrode tips when they are pressed against the Zn-coated (galvanized) surfaces during the resistance spot welding operation. This also contributes to its better electrical and thermal conductivity. The byproducts of these properties are that galvanized steels generally require higher welding currents to be applied for longer times to produce minimum sized welds required by typical automotive component designs [2,3]. Compared to their use on bare steels, resistance spot welding electrodes are undoubtedly exposed to higher temperatures with galvanized steels. Temperatures high enough to melt the Zn (> 420°C), and possibly even to vaporize it (> 906°C), are typically observed [2,3,4,5]. The combination of relatively higher temperatures and contact with liquid Zn are responsible for their accelerated deterioration.

The process of electrode deterioration occurs through a combination of deformation and chemical attack or alloying between the Zn and Cu electrode alloys [2,4]. The behavior of Zn at electrode/sheet metal interfaces has been the subject of numerous studies [2-6,7,8,9,10,11]. It is well established that chemical reactions and mass transport occur between Zn coatings and Cu electrodes. The reactions result in pitting and the formation of Cu-Zn alloy layers on the electrode faces. The α, β, and γ brass phases may all be observed on electrode tips depending on parameters such as welding current, welding time, squeeze pressure, and chemical composition of the Zn layers. These layers will alter the mechanical properties at the electrode faces and they will reduce the melting temperatures of Cu electrode alloys. Deterioration of electrodes used on galvanized steels invariably has been associated with Zn-Cu chemical

reactions. In contrast, fewer studies have considered the possible contributions of deformation to deterioration of electrodes [2,4,11,12]. Whereas the effects of chemical reactions are always present, the independent effects of deformation are more difficult to illustrate. Some work suggests that deformation is unimportant in electrode deterioration on galvanized steels [4]. Other work presents compelling evidence suggesting that deformation could play a dominant role in electrode deterioration, even in the presence of Zn effects [2,11]. Also, few attempts have been made to relate deterioration processes to the intrinsic properties of electrode alloys [2,6,11]. The exact mechanisms of electrode deterioration and the relative contributions of alloying and deformation are still not fully understood. Some of the features of both deformation and chemical attack are schematically illustrated in Figure 1.

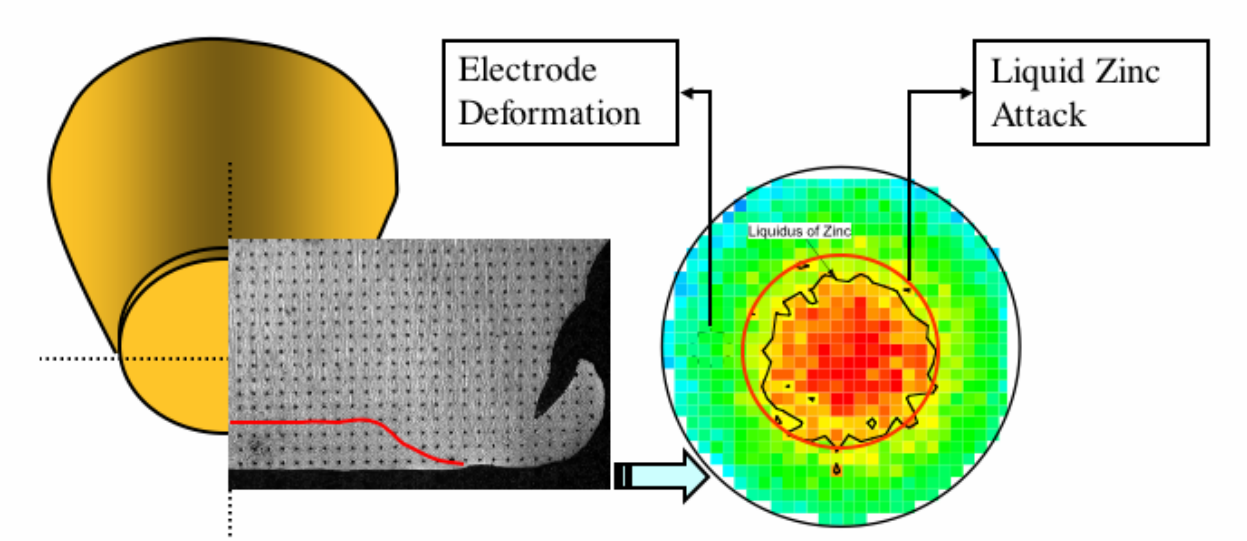

Figure 1. Schematic illustration of copper electrode wear mechanisms through deformation and chemical attack

The work presented here represents an attempt to directly relate resistance spot welding electrode deterioration to electrode properties. It is possible to do this in a fairly rigorous manner using the finite element approach, and simulation of single spot welding events has been done many times to examine various aspects of the process and how they relate to nugget development [9,12,13,14,15,16]. Finite element analysis has even been used to examine electrode deformation over the course of 15 consecutive welds [12]. However, using finite element analysis to effectively analyze electrode deterioration would require successive application of the technique perhaps several thousand times. There are major drawbacks with doing this. One is that the simulation for each spot weld can take up to 10 hrs of computing time. Consequently, the simulation of 2000 spot welds would require about 833 days of computing time! Another problem is that the electrode shape will change with each successive weld. The new electrode shape will require a new mesh, and this is another time-consuming activity. Therefore, applying finite element analysis is not an efficient solution in terms of time and cost for optimizing either electrode materials or geometries over wide ranges of process conditions.

The approach taken in this study was to develop phenomenological models that captured the essential physical processes associated with deformation and chemical attack through analytical models. The strains in the Cu electrode at the electrode/sheet interface during one spot weld were estimated using an analytical deformation model that accumulated strains associated with subsequent spot welds. The amount of strain in each spot weld was related to the stress-strain characteristics of a Cu electrode alloy and its tempering behavior. Chemical effects are considered through a diffusion controlled growth model assuming that the Cu electrode tip is in contact with an infinite reservoir of liquid Zn. Appropriate temperature dependencies are included for analysis of both deformation and chemical attack. The models provide a framework for systematic evaluation of the relationships of electrode deterioration to electrode properties and welding parameters. They run on a personal computer in relatively short times. We believe they are valuable for considering different electrode alloys and for optimizing weld parameters for various industrial conditions.

DEVELOPMENT OF DEFORMATION MODEL

The results from an electrode life test conducted according to AWS D8.9 are shown in Figure 2. The data show that as the number of spot-welds increases the electrode face diameter also continuously increases. Since the welding current is kept constant in these tests, the increase in electrode face diameter leads to a reduction in current density. Eventually the current density is reduced below the critical value needed to produce the required minimum weld button size. This event signals the end of electrode life.

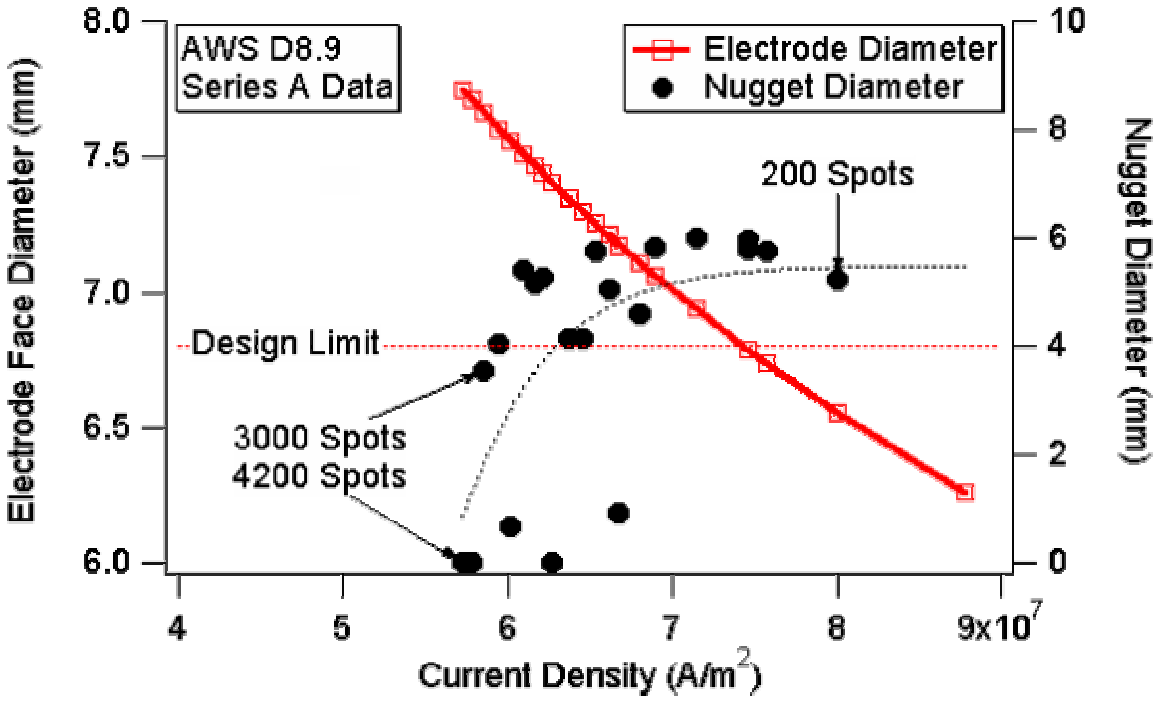

Figure 2. Experimentally measured electrode face diameter and weld nugget diameter as a function of current density during AWS D8.9 test of a class 2 electrode alloy

Figure 2 illustrates the importance of current density on electrode life. It is well known that the current density is directly related to the peak temperatures achieved at the sheet/sheet and electrode/sheet interfaces. The electrode face temperatures will decrease with increasing electrode face diameter for a fixed current level. The face temperature will determine the rates of deformation and chemical attack at the electrode/sheet interface. Therefore, an analytical model was needed to relate the electrode face diameter to electrode face temperature.

Prediction of Electrode Face Temperature

Although, sophisticated finite element or finite difference methods can be used to estimate these temperatures [13,14,15,16,17], to allow for rapid calculations, an empirical sigmoidal equation was used to relate the electrode face temperature (*T*, in Kelvin) to electrode face diameter (*d*, in mm) which is given below.

$$T = 273 + \frac{1358 - 273}{1 + \exp\left[-4.8 + 7.5((d-1)/(10-1))\right]}; I = 10800A \quad (1)$$

The sigmoidal equation allowed the temperature to remain constant close to the melting point of Cu (1358 K) above a certain critical current density. The above equation was compared with a simple finite difference model [18] calculation in Figure 3. The predictions from Equation 1 were in good agreement with the finite difference model in the low temperature regime. Although, the finite difference model captured the spatial variation of temperatures across the electrode face as shown in the inset of the graph, to allow for simplicity Equation 1 ignored the spatial variations of temperature.

Measurement of Electrode Tensile Properties

The increase in face diameter has been related to the deformation characteristics of the Cu electrode face material [2,6,11]. Consequently, any description of electrode deformation will require that some information about the temperature dependence of the mechanical properties of electrode alloys must be known. The tensile properties of CuCrZr class 2 electrode alloy were measured as a function of temperature to provide input for the deformation analysis. The specimens had gage dimensions of 6.35 mm diameter x 31.75 mm length. They were tested at a nominal strain rate of 6.7×10^{-4} s^{-1}. All of the elevated temperature tests were conducted in still air. Typically, it took about 30 minutes to heat to the testing temperature, and another 30 min for the specimen temperature to equilibrate. Thermocouples were affixed to the specimens at each end of their gage lengths and at their centers. Temperature variations along the gage lengths were typically less than 2°C before testing. The results from the tensile testing are presented in Table 1. All of the tensile properties varied significantly with test temperature except for the strain hardening exponent, *n*.

For analysis purposes, the measured true stress-strain characteristics were fitted to the well known equation [19]:

$$\sigma = k\varepsilon^n \tag{2}$$

In this expression, σ corresponds to true plastic stress, ε is the strain above the proportional limit, *k* is the coefficient of the stress and *n* is the strain hardening exponent.

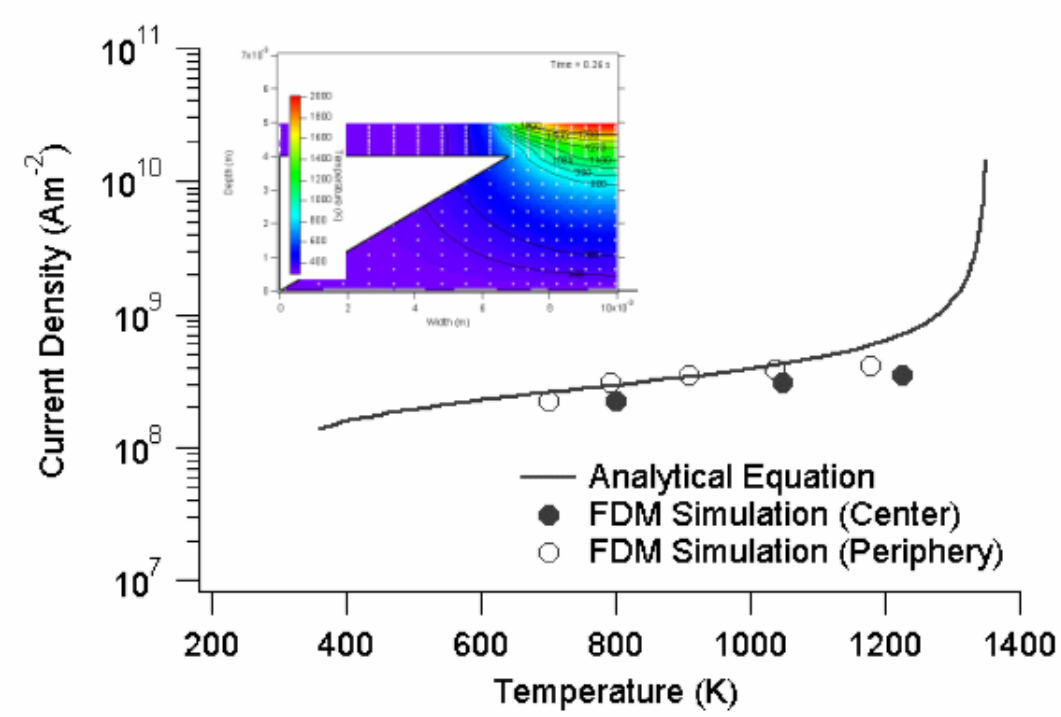

Figure 3. Predicted variation of electrode face temperature with Equation 1 for different current density levels. Inset shows the typical temperature variation predicted by a finite difference model.

Table 1. Summary of tensile properties for CuCrZr class 2 electrode alloy

Test temp., °C	Proportional limit, MPa	0.2% Y.S., MPa	U.T.S., MPa	Uniform elong., %	Hardening Exponent
25	360.0	592.1	619.2	0.51	0.106
200	313.0	513.0	532.9	0.45	0.105
300	226.8	452.3	467.7	0.46	0.128
400	224.4	381.7	392.3	0.45	0.144
500	191.9	308.8	317.2	0.46	0.091
600	63.9	194.4	211.8	0.60	0.198
700	30.6	46.3	49.2	2.77	0.058
800	10.8	23.1	24.2	1.48	0.108

Progressive electrode deformation

Equation 2 assumes that the electrode material does not degrade with number of welds, i.e., that there is no time dependence of tensile properties. However, regions of the electrodes near their faces will soften due to repeated heating and cooling during welding operations [2,11]. The spatial variation of Vickers microhardness of the CuCrZr electrode alloy was also measured at various stages of electrode life [20], and microhardness maps are presented in Figure 4. The maps were done on only one half of the sectioned surfaces because of axial symmetry. Figure 4*a* shows that the hardness of the electrode alloy near the tip was 120 kg/mm^2 after 100 welds, while the bulk of the electrode exhibited a hardness of 180 kg/mm^2. This confirms that softening occurs fairly rapidly in the cold worked, precipitation hardened electrode alloy as has been observed in other work [11]. The hardness distributions after 500 welds and at the end-of-life stage are shown in Figure 4*b* and *c*. As life testing proceeded, microhardness values near the electrode tip fell to as low as 70 kg/mm^2. However, the hardness distribution did not change significantly after 500 welds. These results demonstrate that an assumption of constant room temperature strength in a deformation model for electrode alloys is not valid. Therefore, the following material degradation equation was developed to describe the variation of proportional limit and *k* with number of spot welds:

$$\sigma_{YS}^{RT}\Big|_i = \text{Ratio}_A \times \sigma_{YS}^{RT}\Big|_o + \text{Ratio}_B \times \sigma_{YS}^{RT}\Big|_o \times \exp\left\{-i/k_{decay}\right\} \quad (3)$$

In this equation, Ratio_A and Ratio_B define the extent of softening and k_{decay} defines the rate of softening and *i* is the number of spot welds. Typical values of these parameters used in this research are: $\text{Ratio}_A = 0.3337$; $\text{Ratio}_B = 0.6667$ and $k_{decay} = 500$. A typical reduction in yield strength with number of spot welds is shown in Figure 5. It is important to note that these parameters will depend on the metallurgical stability of the electrode alloys to be used in the model. Ultimately, this analysis predicts that copper alloys which are more resistant to softening processes such as recovery and recrystallization will have improved resistance to continuous deformation during welding operations.

Coupled Deformation Model

The descriptions of temperature variation at the electrode face, temperature-dependent tensile properties, and softening behavior were then combined into a simple model of electrode deformation. The model assumes that the deformation is confined to a disc of material at the electrode tip. The initial diameter of the disc is that of the electrode tip, and it will enlarge with each successive application of welding force, *F*, i.e., with each welding event. However, the rate at which the disc diameter, *d*, enlarges will continuously decrease because the area supporting the welding force continuously increases. The tensile properties and softening characteristics will also influence the rate of disc enlargement. Initially, the pressure associated with *F* exceeds the yield stress of the electrode alloy at the temperature of the disc. The deformation of the disc will eventually cease when the pressure associated with *F* equals the yield strength of the alloy. At that point, mechanical equilibrium is achieved at the electrode face. This process is shown schematically in Figure 6. The increase in the electrode face diameter as given by:

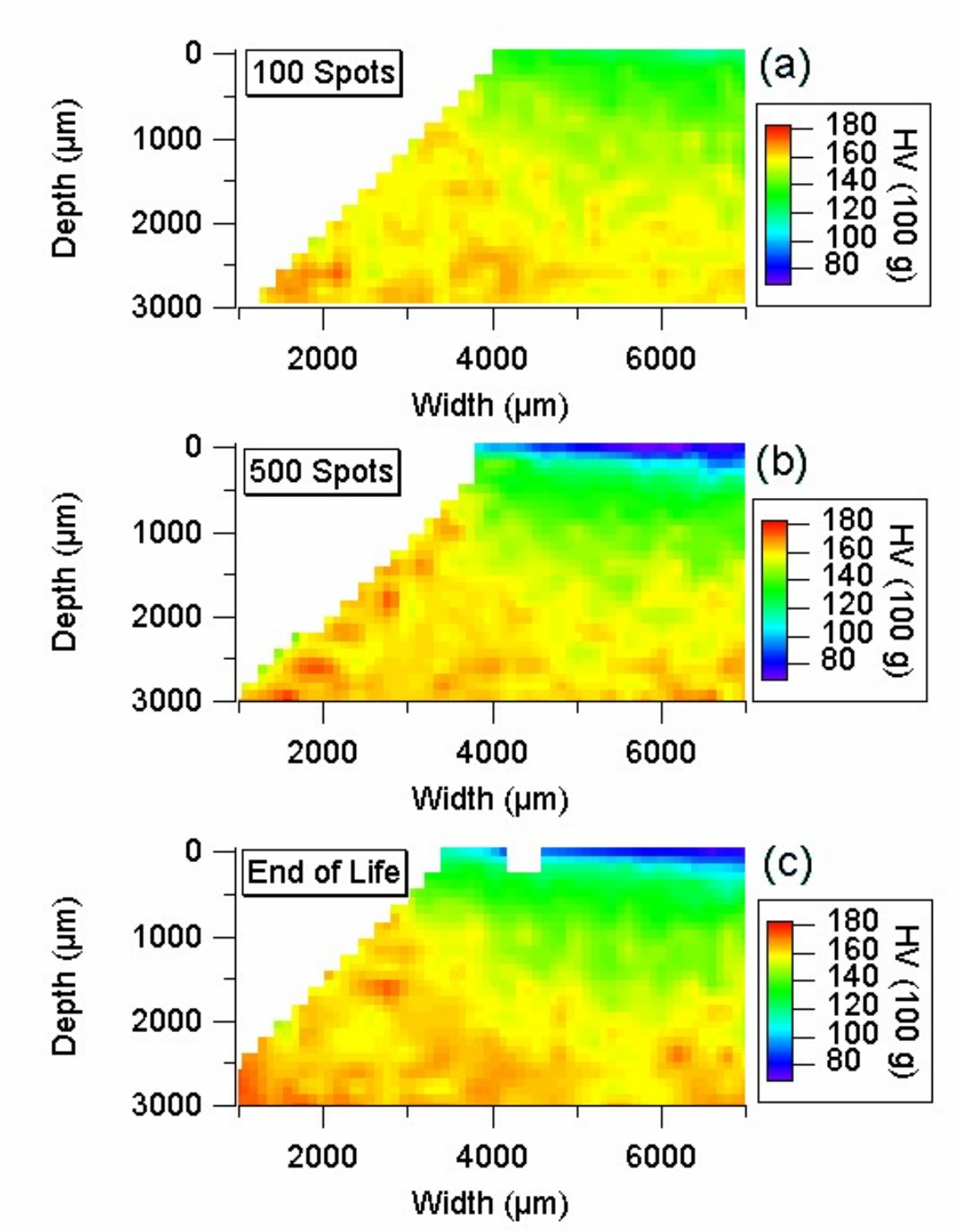

Figure 4. Measured spatial variation of hardness in copper electrodes after (*a*) 100 welds, (*b*) after 500 welds, and (*c*) at the end of life shows progressive softening at the electrode face.

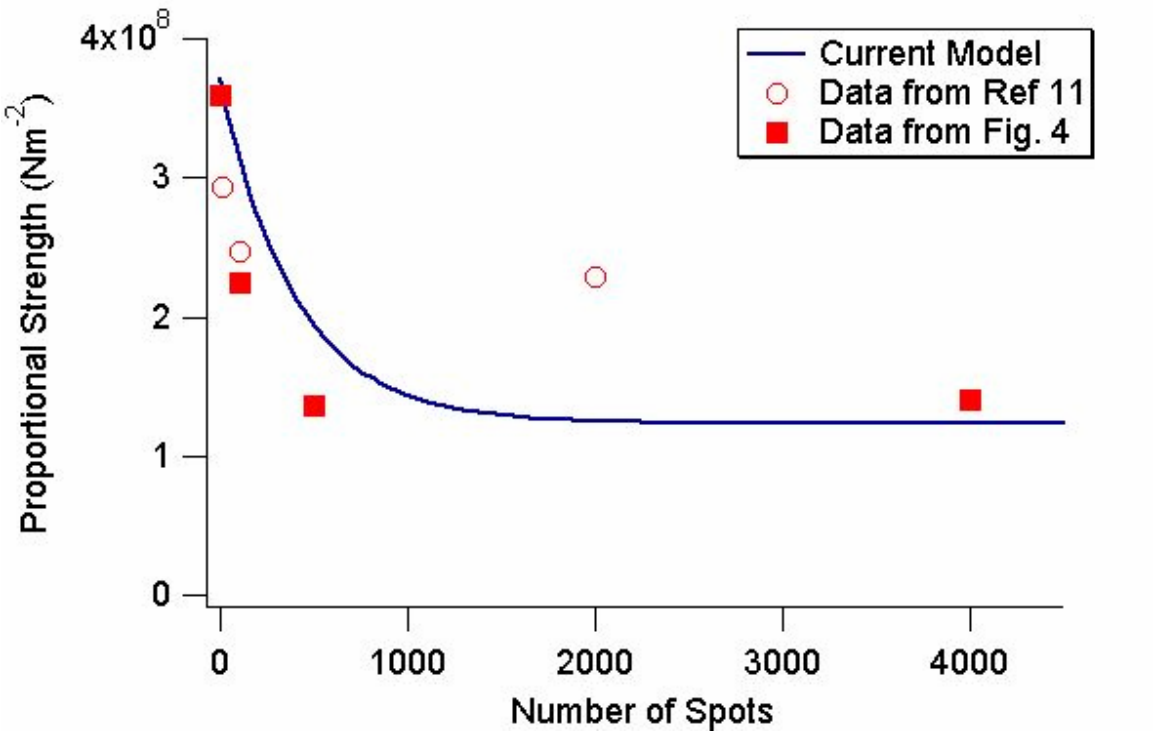

Figure 5. Calculated variation of proportional strength with number of spot welds for conditions mentioned in the text

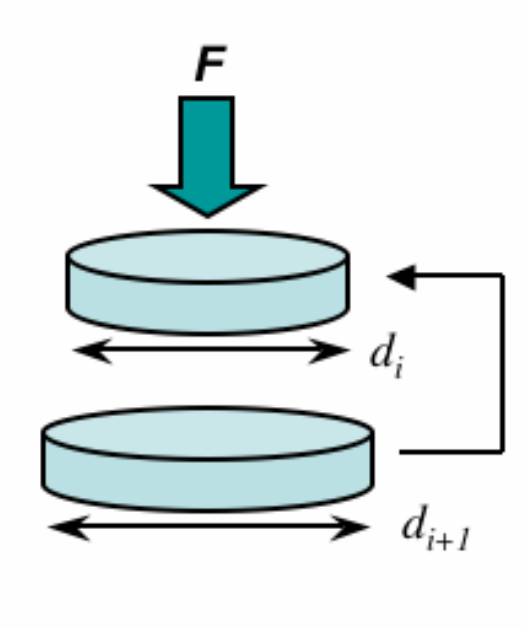

Figure 6. Schematic illustration of disc deformation model

$$\frac{\Delta d}{d} = \varepsilon = \left[\frac{4F/\left(\pi d_i^2\right)}{K}\right]^{\frac{1}{n}}; d_{i+1} = d_i\left[1+\varepsilon\right] \quad (4)$$

While this expression ignores many of the intricacies of the mechanical deformation process, it does provide a straightforward means to describe strain accumulation at electrode tips that depends on well established materials behaviors. Also, calibration of the equation with experimental data is required to establish a realistic reference point for further analysis of electrode deformation behavior.

Evaluation of the Model

The deformation model represented by Equation 4 was fit to experimental measurements to establish the necessary reference condition as shown in Figure 7. This general approach to describing electrode deterioration has been taken by others [12, 21]. However, the present method allows for systematic evaluation of how electrode alloy properties and welding parameters influence the growth of electrode tips.

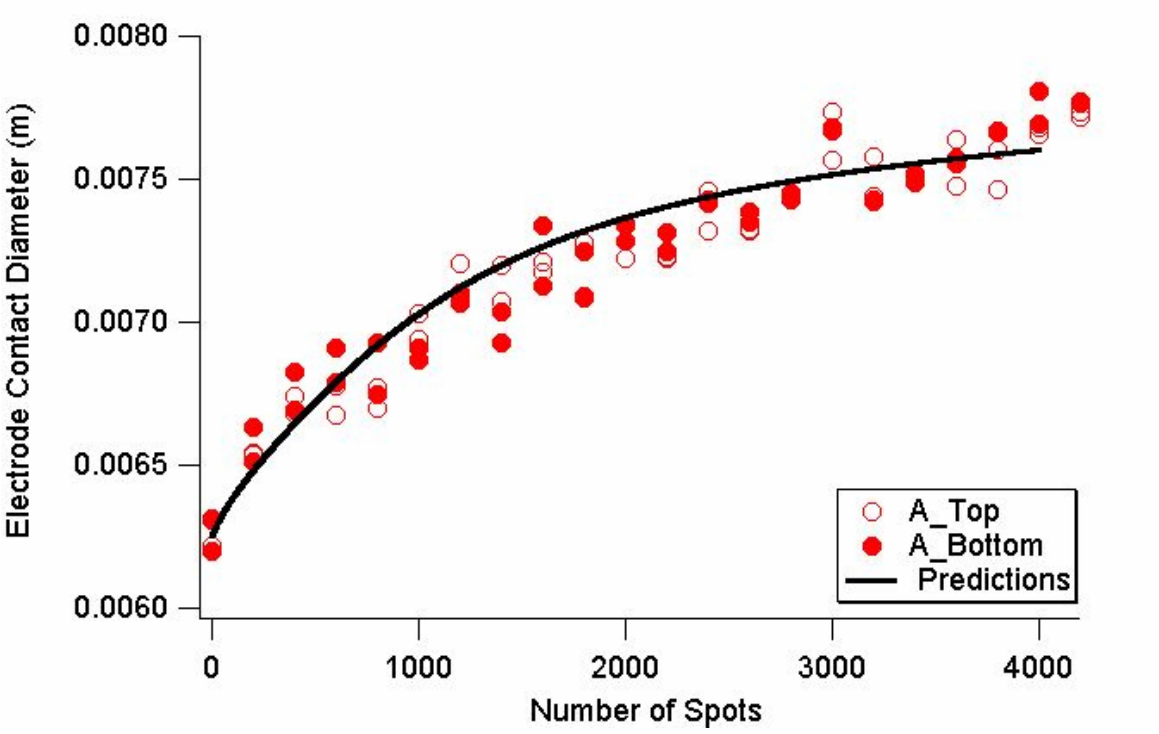

Figure 7. Comparison of predictions using Equation 4 and experimentally measured face diameters from top and bottom electrode as a function of number of welds during AWS D8.9 test for A-type electrodes

The results of using the deformation model to consider changes to electrode alloy properties are shown in Figure 8. Two modifications to the reference electrode properties are illustrated. In the first, for the same electrode tensile properties given in Table 1, the softening resistance was increased. This was done by changing the k_{decay} to 5000 from the reference value of 500. The

prediction suggests that the increase in softening resistance virtually eliminates the initial rapid growth stage of electrode tip deformation producing an nearly steady state growth condition from the start of the life behavior. In the second case, the high softening resistance was maintained, but the alloy strength was reduced over the entire temperature range. These hypothetical conditions produced a deformation rate that was initially high. However, the predicted deformation rate also quickly approached a steady state.

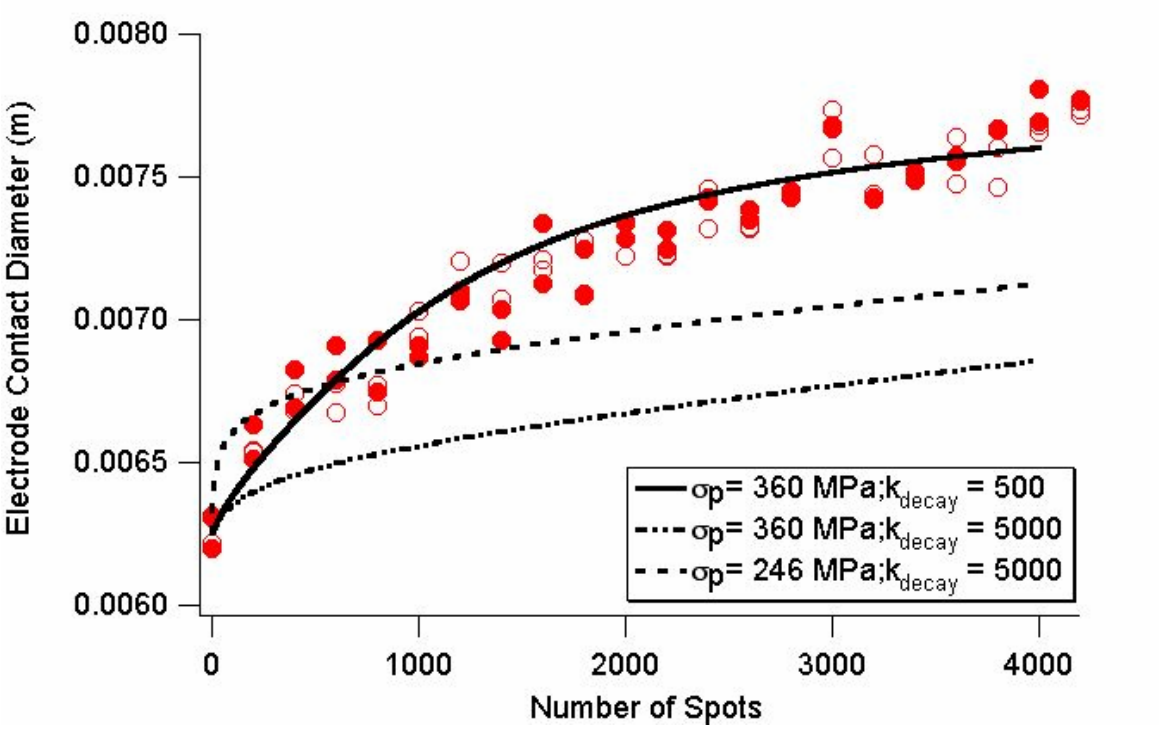

Figure 8. Predicted variations of electrode face diameter for different electrode properties as a function of number of spot welds compared to the model reference condition

The results of using the deformation model to evaluate the effects of varying the welding current are shown in Figure 9. Two hypothetical conditions of either a 1 kA increase or a 1 kA decrease in welding current are compared to the reference condition of 10.8 kA. As expected, an increase in welding current accelerated the electrode tip growth below about 1500 welds. The decrease in welding current is predicted to suppress electrode tip deformation initially. After a few hundred welds, however, the deformation behavior is similar to the reference condition but a smaller face diameter is predicted for the same number of welds. These hypothetical demonstrations illustrate the utility of the present model to evaluate wide range of electrode materials and welding process parameters to predict electrode wear.

There is no question that this model greatly simplifies the mechanical and metallurgical issues associated with the electrode deformation process. However, as details are added to improve technical precision, the complexity of the analysis and the demand for computation time increases. Our intention was to provide a engineering tool that would be capable of guiding electrode alloy development efforts and selecting welding parameters, and one that was

relatively accessible to a wide range of potential users. This personal–computer-based deformation model satisfies that objective.

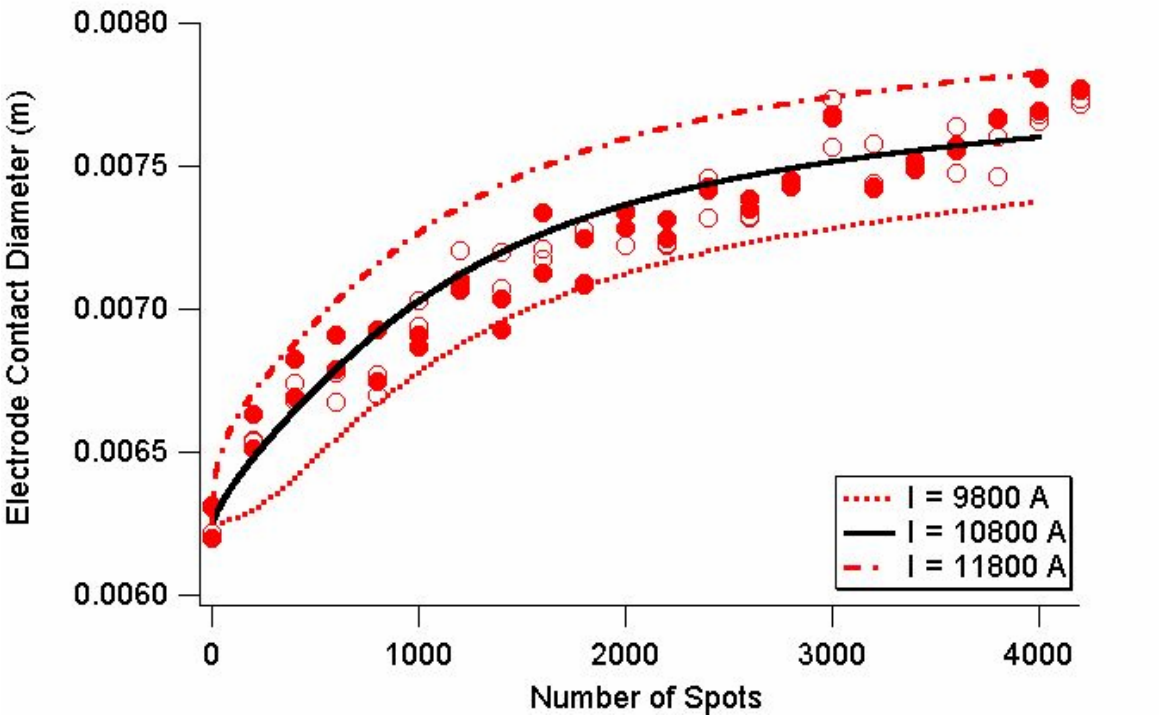

Figure 9. Predicted variations of electrode face diameter for different welding current values as a function of number of spot welds compared to the model reference condition

DEVELOPMENT OF CHEMICAL ATTACK MODEL

Clearly any general model of resistance spot welding electrode deterioration must account for chemical attack mechanisms. This aspect of electrode deterioration is being addressed through application of diffusion controlled growth analysis. One dimensional diffusion (analogous to the axial direction in an electrode tip) in a material couple between Cu and Zn is being considered. The chemical activity of Zn at the Cu/Zn interface is held constant at unity, which is equivalent to assuming there is an infinite reservoir of Zn. This is reasonable for describing conditions over typical electrode lives of 1000s of welds.

The formation of liquid Zn at the Zn/Cu interface is permitted based on thermodynamic stability criteria. The simulation geometry is schematically shown in Figure 10. Two simulation conditions are considered: (1) a peak temperature close to the melting point of Zn, and (2) a peak temperature above the melting point of Zn. The analyses are based on somewhat arbitrary temperature profiles with durations of 0.5 s. The calculations were performed with DicTra™ software [22] assuming a diffusivity of Cu in liquid Zn of 10^{-8} m^2/s.

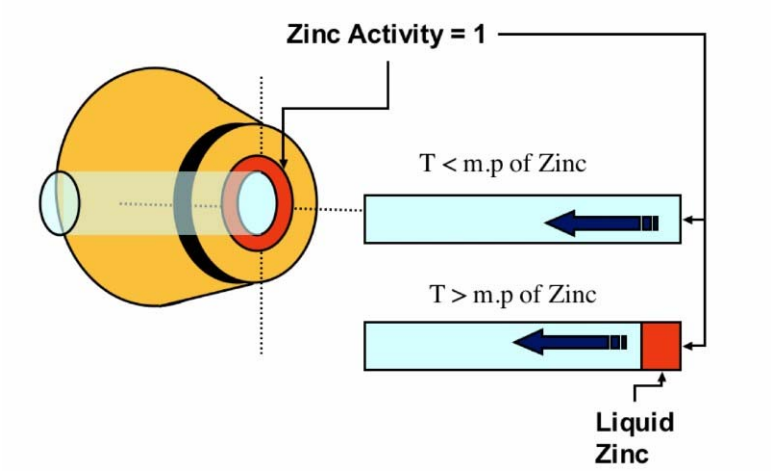

Figure 10. Schematic illustration of geometry used for diffusion controlled growth model.

The results are presented in Figure 11. The case where the Zn does not melt was based on the thermal cycle shown in Figure 11*a* in which the temperature increases from room temperature to near the melting point of Zn (693 K) in 0.4 s and cools back to room temperature in 0.1 s. Because Zn does not melt only solid-state diffusion occurs across this Cu/Zn interface and the profile of Zn concentration in the Cu is shown in Figure 11*b*. For these conditions, the diffusion distance for Zn into the Cu is less than 1 nm, a miniscule amount. The thermal cycle for the case where Zn melting is permitted is shown in Figure 11*c*. The initial temperature is just above 693 K. It increases to a maximum of 1000 K in 0.4 s, and then decreases back to 693 K in 0.1 s. For these conditions Cu dissolves into the Zn and the Cu/Zn interface rapidly penetrates into the Cu. The profiles for Zn penetration into the Cu are shown in Figure 11*d* for this case. The maximum extent of the Zn penetration was about 500 nm. These results are consistent with the conclusion that it is the reaction of liquid Zn with Cu alloy electrode tips that dominates the chemical attack process [2,3,4,11]. Subsequent solidification of the Cu-rich liquid at the Cu/Zn interface will result in the formation of brass layers on the electrode tip.

A simple melting experiment was done to illustrate the rate of reaction between liquid Zn and Cu. An OFHC Cu specimen with dimensions of 12 x 12 x 3 mm was heated in high purity argon atmosphere to 440°C on a hot plate with digital temperature control. A 0.25 g pellet of high purity Zn was then place on the Cu. The Zn melted within several seconds, and then the specimen was removed from the hot plate and rapidly cooled to room temperature. The total contact time between the liquid Zn and Cu could not be accurately determined, but it was very brief, less than 30 s. An optical micrograph of the Zn droplet that solidified on the Cu surface is shown in Figure 12*a*. Reaction of the Zn with the Cu surface is illustrated in Figure 12*b* where the original position of the Cu surface is indicated by the dotted line. Penetration of the liquid Zn into the Cu surface is evident. Also, diffusion of Zn into the Cu is indicated by the yellow layer of α-brass. Identical results were obtained when this experiment was repeated using CuCrZr rather than OFHC Cu.

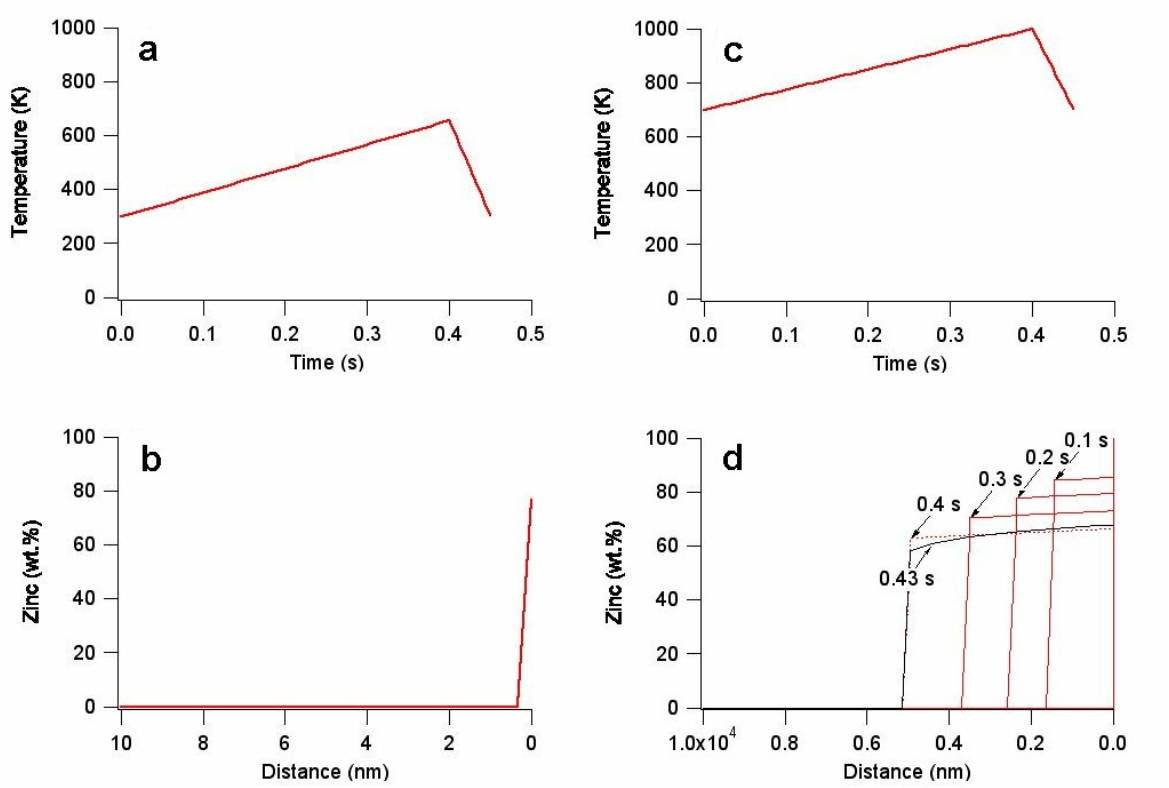

Figure 11. (a) Assumed temperature profile with a peak temperature lower than melting point of zinc and (b) calculated solid-state diffusion profile in the copper block. (c) Assumed temperature profile with a peak temperature higher than melting point of zinc and (d) calculated penetration depth of liquid zinc into copper block.

Analysis of the chemical aspects of electrode deterioration are continuing with one objective being development of a predictive capability similar to the deformation model. Whether deformation or chemical attack dominates deterioration is not clear [2,4,6,11]. Certainly both deterioration mechanisms are operating in resistance spot welding electrodes, and either could be dominant under specific welding conditions or during different periods of the typical electrode life behavior. For instance, in the early period of life, electrode diameters are relatively small resulting in relatively high current densities and contact pressures. The higher current densities will increase temperatures at the electrode/sheet interfaces and this will promote deformation. Higher contact pressures will also make deformation at the electrode tip more likely. In later life, as face diameters enlarge current densities and contact pressures will decrease, thereby reducing the probability of further deformation. In contrast, the formation of liquid Zn at electrode/sheet interfaces is likely to occur irrespective of electrode tip diameter. Consequently, it may be that deformation is more important as an electrode deterioration mechanism in the early stages of life, while chemical attack is nearly constant throughout. Developing an improved generalized model of electrode deterioration, even of a simplified variety like the present case, will require a better understanding of the deterioration mechanisms and their interrelationships.

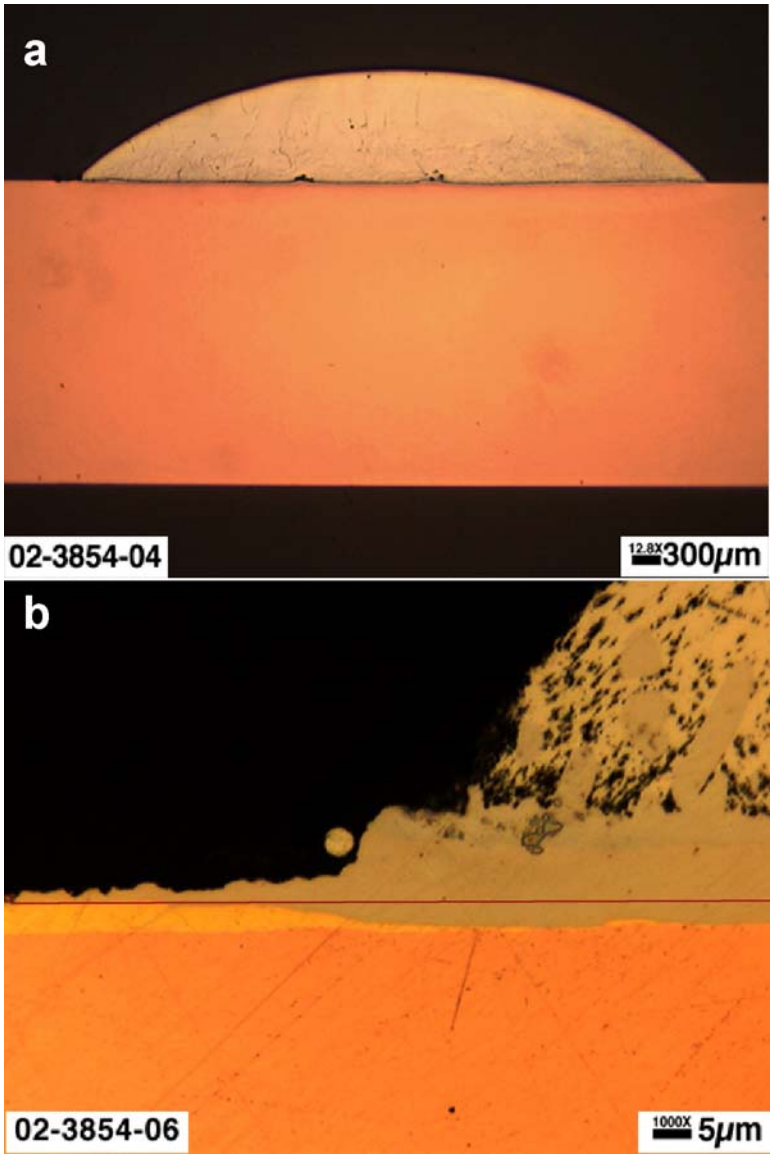

Figure 12. (a) Macrograph showing the presence of solidified zinc layer on top of the copper electrode and (b) high magnification micrograph showing thee presence of different brass layers with different colors indicating different Zn concentrations

CONCLUSIONS

An analytical model that relates the electrode face diameter, welding load, welding current, mechanical properties as a function of temperature, and material degradation to electrode wear was developed. The model suggested that the life of resistance spot welding electrodes can be increased by enhancing their softening resistance rather than their absolute strength. A diffusion controlled growth model showed that if the electrode face temperature is higher than melting point of Zn, there is a probability of significant penetration of liquid Zn into Cu. The predicted rate of liquid Zn penetration into Cu was 500 times more than the rate of solid-state diffusion. Melt drop experiments confirmed that liquid Zn penetration into Cu readily occurs and will lead to the formation of different brass reaction layers.

ACKNOWLEDGEMENTS

The research was sponsored by the Assistant Secretary for Energy Efficiency and Renewable Energy, Office of FreedomCAR and Vehicle Technologies, as part of the Automotive Lightweighting Materials Program, U. S. Department of Energy, under contract DE-AC05-00OR22725 with ORNL operated by UT/Battelle, LLC. The authors thank Z. Feng and M. Murugananth for reviewing the manuscript.

REFERENCES

1. ASM Handbook, *Volume 2 Properties and Selection: Nonferrous Alloys and Special-Purpose Materials*, 10th Edition, Properties of Pure Metals, ASM International, Materials Park, Ohio, 1990
2. N. A. Freytag, "A Comprehensive Study of Spot Welding Galvanized Steel, *Welding Journal*, vol. 44, no. 4, 1965, pp. 145-s-156-s
3. P. Howe and S. C. Kelley, "A Comparison of the Resistance Spot Weldability of Bare, Hot-Dipped, Galvannealed, and Electrogalvanized DQSK Sheet Steels," SAE paper 880280, 1988
4. W. R. Upthegrove and J. F. Key, "A High Speed Photographic Analysis of Spot Welding Galvanized Steel," *Welding Journal*, vol. 51, no. 5, 1972, pp. 233-s-244-s.
5. S. A. Gedeon and T. W. Eagar, *Metallurgical Transactions B*, vol. 17B, no. 12, 1986, pp. 887-901.
6. K. I. Johnson, "Spot Welding Electrode Life Tests on Galvanized Steel Sheet," *The Welding Institute Research Report*, P/74/75, November, 1975
7. S. Mathieu and P. Patou, "Zinc Coating Influence on Spot-Weldability of Hot-Dip Galvanized Steel Sheets," SAE paper 850273, 1985
8. R. Holliday, J. D. Parker, and N. T. Williams, "Electrode deformation when spot welding coated steels," *Welding in the World*, vol. 35, no. 3, 1995, pp. 160-164
9. A. De, L. Dorn, and O. P. Gupta, "Analysis and optimization of electrode life for conventional and compound tip electrodes during resistance spot welding of electrogalvanized steels," *Science and Technology of Welding and Joining*, vol. 5, no. 1, 2000, pp. 49-57
10. M. Kimchi, M. D. Gugel, and C. L. White, "Mechanisms of Electrode Wear During Resistance Spot Welding Hot-Dipped Galvanized Steel," *Cooperative Research Program Summary Report SR0009*, EWI, Columbus, Ohio, 2000.
11. J. D. Parker, N. T. Williams, and R. J. Holliday, "Mechanisms of electrode degradation when spot welding coated steels," *Science and Technology of Welding and Joining*, vol. 3, no. 2, 1998, pp. 65-74
12. P. Dong, M. V. Li, and M. Kimchi, "Finite element analysis of electrode wear mechanisms: face extrusion and pitting effects," *Science and Technology of Welding and Joining*, vol. 3, no. 2, 1998, pp. 59-64
13. H. A. Nied, "The Finite Element Modeling of the Resistance Spot Welding Process," *Welding Journal*, vol. 63, no. 4, 1984, pp. 123-s-132-s
14. C. L. Tsai, O. A. Jammal, J. C. Papritan, and D. W. Dickinson, "Modeling of Resistance Spot Welding Nugget Growth," *Welding Journal*, vol. 71, no. 2, 1992, pp. 47-s-54-s
15. H. S. Cho and Y. J. Cho, "A Study of the Thermal Behavior in Resistance Spot Welds, *Welding Journal*, vol. 68, no. 6, 1989, pp. 236-s-244-s.
16. Z. Feng, J. E. Gould, S. S. Babu, M. L. Santella, and B. W. Riemer, "An Incrementally Coupled Electrical-Thermal-Mechanical Model for Resistance Spot Welding," pp. 599-604

in *Trends in Welding Research, Proceedings of the 5th International Conference*, edited by J. M. Vitek, S. A. David, J. A. Johnson, H. B. Smartt, and T. DebRoy, ASM International, Materials Park, Ohio, 1999
17. J. E. Gould, “An Examination of Nugget Development during Spot Welding, Using Both Experimental and Analytical Techniques,” *Welding Journal*, vol. 66, no. 1, 1987, pp. 1-s-10-s.
18. S. S. Babu, unpublished research, Oak Ridge National Laboratory, 2003
19. *Mechanical Metallurgy*, Third Edition, G. E. Dieter, McGraw-Hill, 1986, pp. 287-288
20. R. J. Bowers work, this proceedings
21. F. Lu and P. Dong, “Model for estimating electrode face diameter during resistance spot welding, *Science and Technology of Welding and Joining*, vol. 4, no. 5, 1999, pp. 285-289
22..J.-O. Andersson, L. Höglund, B. Jönsson and J. Agren, “Computer simulations of diffusional transformations in steel,” pp. 153-163 in *Fundamentals and applications of ternary diffusion*, edited by G. R. Purdy, Pergamon Press, 1990